

# Lattice dynamics of the infinite-layer nickelate $\text{LaNiO}_2$

Shohei Hayashida,<sup>1,2,\*</sup> Vignesh Sundaramurthy,<sup>2</sup> Wenfeng Wu,<sup>3,4</sup> Pascal Puphal,<sup>2</sup> Thomas Keller,<sup>2,5</sup> Björn Fåk,<sup>6</sup> Masahiko Isobe,<sup>2</sup> Bernhard Keimer,<sup>2</sup> Karsten Held,<sup>7</sup> Liang Si,<sup>8,†</sup> and Matthias Hepting<sup>2,5,‡</sup>

<sup>1</sup>*Neutron Science and Technology Center, Comprehensive Research Organization for Science and Society (CROSS), Tokai, Ibaraki 319-1106, Japan*

<sup>2</sup>*Max-Planck-Institute for Solid State Research, Heisenbergstraße 1, 70569 Stuttgart, Germany*

<sup>3</sup>*Key Laboratory of Materials Physics, Institute of Solid State Physics, HFIPS, Chinese Academy of Sciences, Hefei 230031, China*

<sup>4</sup>*Science Island Branch of Graduate School, University of Science and Technology of China, Hefei 230026, China*

<sup>5</sup>*Max Planck Society Outstation at the Heinz Maier-Leibnitz Zentrum (MLZ), Lichtenbergstraße 1, 85748 Garching, Germany*

<sup>6</sup>*Institut Laue-Langevin, 71 Avenue des Martyrs, 38042 Grenoble Cedex 9, France*

<sup>7</sup>*Institut für Festkörperphysik, Technische Universität Wien, 1040 Wien, Austria*

<sup>8</sup>*School of Physics, Northwest University, Xi'an 710127, China*

(Dated: September 5, 2025)

Infinite-layer (IL) nickelates have rapidly emerged as a new class of superconductors. However, due to the technical challenges of their topotactic synthesis, they have so far been realized primarily as thin films or polycrystalline powder samples, limiting comprehensive investigations of fundamental physical properties such as the lattice dynamics. Here, we present a time-of-flight inelastic neutron scattering study on a sample composed of a large number of co-aligned bulk crystals of the IL nickelate  $\text{LaNiO}_2$ . We observe several dispersive phonon branches, which are in good agreement with lattice dynamical calculations based on density-functional perturbation theory. In addition, we compare the characteristics of selected  $\text{LaNiO}_2$  phonon modes to those of isostructural cuprate superconductors. Our findings provide a reference point for future experimental and theoretical efforts aimed at understanding the interplay between lattice dynamics and electronic properties in IL nickelates.

## I. INTRODUCTION

The recent discovery of superconductivity in infinite-layer (IL) nickelates [1] has generated significant interest due to their structural and electronic similarities to high-temperature superconducting cuprates. In the latter, superconductivity emerges upon doping charge carriers into the  $\text{CuO}_2$  planes, thereby suppressing the long-range antiferromagnetic order of the parent Mott-insulating state [2–5]. Nevertheless, despite decades of intensive research, consensus on the microscopic mechanism underlying unconventional superconductivity in cuprates remains elusive. Therefore, the discovery and exploration of related materials, such as IL nickelates, which might share key superconducting characteristics, offers promising opportunities to address this long-standing problem.

Striking similarities between IL nickelates of composition  $R\text{NiO}_2$  ( $R$ : rare-earth ion) and cuprates were pointed out early in theoretical studies [6], even preceding the experimental confirmation of superconductivity in IL nickelate thin films [1, 7–12]. In particular, both material classes exhibit  $\text{NiO}_2$  ( $\text{CuO}_2$ ) planes, wherein  $\text{Ni}^{1+}$  ( $\text{Cu}^{2+}$ ) ions nominally adopt a  $3d^9$  electronic configuration. However, later theoretical studies predicted distinct features of the electronic structure of IL nickelates [13], including a diminished  $3d$ - $2p$  hybridization between Ni

and the O ligands, while at the same time rare-earth  $5d$  Fermi surface pockets self-dope the Ni  $3d$  bands [14–29], which explains the metallic properties of the parent  $R\text{NiO}_2$  compounds. Signatures of this distinct electronic structure of IL nickelates have been evidenced in recent photon and electron-spectroscopic measurements [30–33].

In cuprates, the electronic structure and lattice dynamics are strongly coupled, leading to pronounced anomalies in specific phonon modes [34]. Notably, the Cu–O bond-stretching (breathing) modes exhibit anomalous softening and broadening at characteristic wavevectors, indicative of strong electron-phonon interactions [35–41]. Some of these anomalies, revealed by phonon dispersion measurements using inelastic neutron and x-ray scattering across various cuprate families, have been discussed in the context of the microscopic mechanisms driving charge density wave formation [42]. Phonons thus serve as a sensitive probe of the underlying charge correlations. Consensus holds that spin fluctuations [43, 44] play a central role in the superconducting pairing mechanism in cuprates [45–48], whereas electron-phonon interactions are insufficient to account for the high superconducting transition temperatures, although phonons may still contribute to or interact with the pairing process [49–54].

In superconducting IL nickelates, the pairing mechanism and symmetry remain under investigation. Initial spectroscopic studies on samples with potentially degraded surfaces yielded conflicting results regarding nodal versus fully gapped behavior [55–60], whereas recent ultrafast optical spectroscopy experiments suggest a weak-coupling  $d$ -wave pairing state [61]. Given their

\* [s.hayashida@cross.or.jp](mailto:s.hayashida@cross.or.jp)

† [siliang@nwu.edu.cn](mailto:siliang@nwu.edu.cn)

‡ [hepting@fkf.mpg.de](mailto:hepting@fkf.mpg.de)

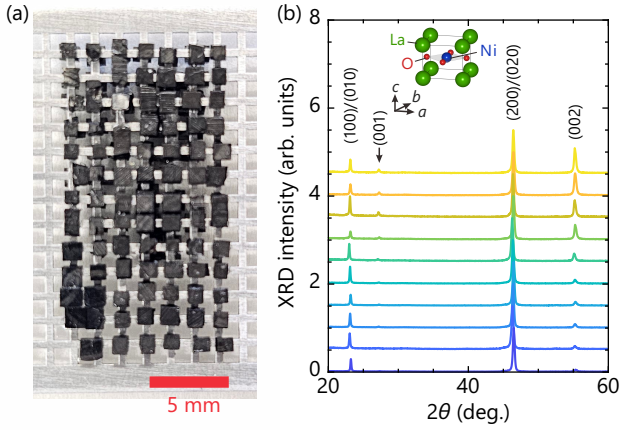


FIG. 1. (a) Sample array with co-aligned  $\text{LaNiO}_2$  crystals on two sides of an Al grid. (b) Representative XRD patterns from the surface of individual  $\text{LaNiO}_2$  crystals, acquired with  $\text{Cu } K_\alpha$  radiation at 300 K. The Bragg peaks are indexed. The inset shows the tetragonal  $P4/mmm$  unit cell of  $\text{LaNiO}_2$ .

moderate superconducting transition temperature ( $T_c \lesssim 20$  K) relative to cuprates [62, 63], the role of phonons and possible lattice instabilities remains an active field of inquiry [64–68]. Theories diverge on this point, suggesting either strong electron-phonon coupling (EPC) [69–71] and phonon-driven  $s$ -wave gap scenarios [70, 72, 73], or that EPC in IL nickelates is insufficient to explain superconductivity [14, 74]. In lieu thereof, spin fluctuations have been suggested as the dominant pairing mechanism [75, 76], similarly to the cases of cuprates and iron-based superconductors [3].

However, in spite of numerous theoretical studies on the lattice dynamics of IL nickelates and continued debate over the role of phonons [64–70, 72, 74, 77–81], a basic experimental characterization of their phonon spectrum is lacking. This is likely due to the demanding nature of the topotactic synthesis process, which previously limited the availability of IL nickelate samples to thin films or polycrystalline powders, preventing the acquisition of highly resolved energy- and/or momentum-dependent spectroscopic data from bulk single-crystals, for instance by inelastic neutron scattering (INS). Additionally, optical spectroscopy has not been able to clearly distinguish phonons in IL nickelate films from substrate contributions [82], and no Raman-active phonon modes exist at the zone center for the  $P4/mmm$  structure of  $\text{RNiO}_2$  [83, 84].

In this work, we perform INS experiments on  $\text{LaNiO}_2$  crystals, observing various branches of acoustic and optical phonons. We compare the measured phonon spectrum to lattice dynamical calculations obtained via density-functional perturbation theory (DFPT) [85] and discuss the computed dispersions in the context of characteristic phonons in cuprates, including bond stretching, buckling, and bending modes as well as charge fluctuation-coupled modes. The results establish a ba-

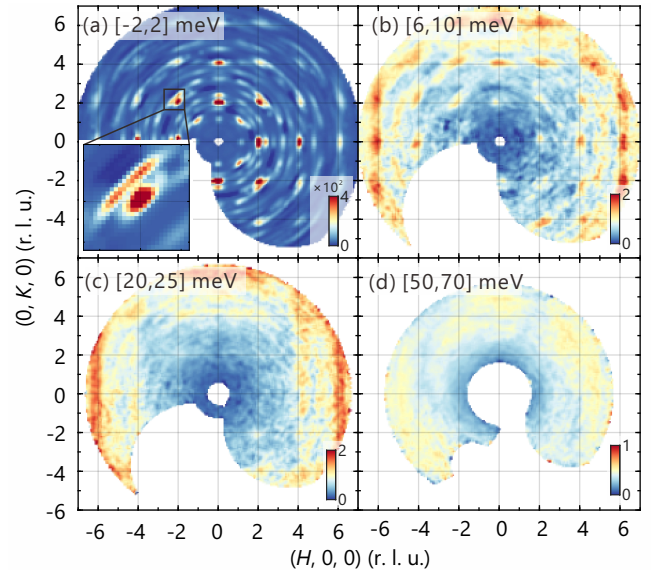


FIG. 2. (a)–(d) Constant energy slices of the INS spectra in the  $(H, K, 0)$  plane for incident neutron energy  $E_i = 76$  meV. The transferred energies are integrated over the following ranges: (a)  $-2 \leq E \leq 2$  meV, (b)  $6 \leq E \leq 10$  meV, (c)  $20 \leq E \leq 25$  meV, and (d)  $50 \leq E \leq 70$  meV. The integration range along the out-of-plane direction is  $\pm 0.37 \text{ \AA}^{-1}$ . The inset in panel (a) highlights two satellite peaks from  $P4/mmm$  twin domains around the  $(-2, 2, 0)$  Bragg peak.

sis for future studies exploring the interplay between lattice dynamics, EPC, and the electronic properties of IL nickelates.

## II. MATERIALS AND METHODS

Cube-shaped  $\text{LaNiO}_2$  crystals with dimensions of approximately  $1 \text{ mm}^3$  were obtained through topotactic reduction of optical floating zone (OFZ) grown  $\text{LaNiO}_3$  crystals [86, 87], using  $\text{CaH}_2$  as the reducing agent. The details of the synthesis procedure are described in Ref. [88]. More than 100  $\text{LaNiO}_2$  crystals with a total mass of 870 mg were co-aligned on an Al grid for the INS experiment [Fig. 1(a)]. X-ray diffraction (XRD) from the surface of individual  $\text{LaNiO}_2$  crystals [Fig. 1(b)] revealed the presence of  $(H, 0, 0)/(0, K, 0)$  and  $(0, 0, L)$ -type Bragg peaks of the tetragonal  $P4/mmm$  space group, suggesting that the crystals contain three twin domains, as described in detail in Ref. [88]. Different intensity ratios between the Bragg peaks in the XRD patterns of different crystals [Fig. 1(b)] indicate that each crystal might exhibit a distinct domain population across the probed surface region. In the INS experiment which picks up the bulk signal from the entire sample array consisting of more than 100 crystals, the varying domain populations are averaged out see Supplementary Information [89]) and we assume an equal population of the three domains for the INS data analyses.

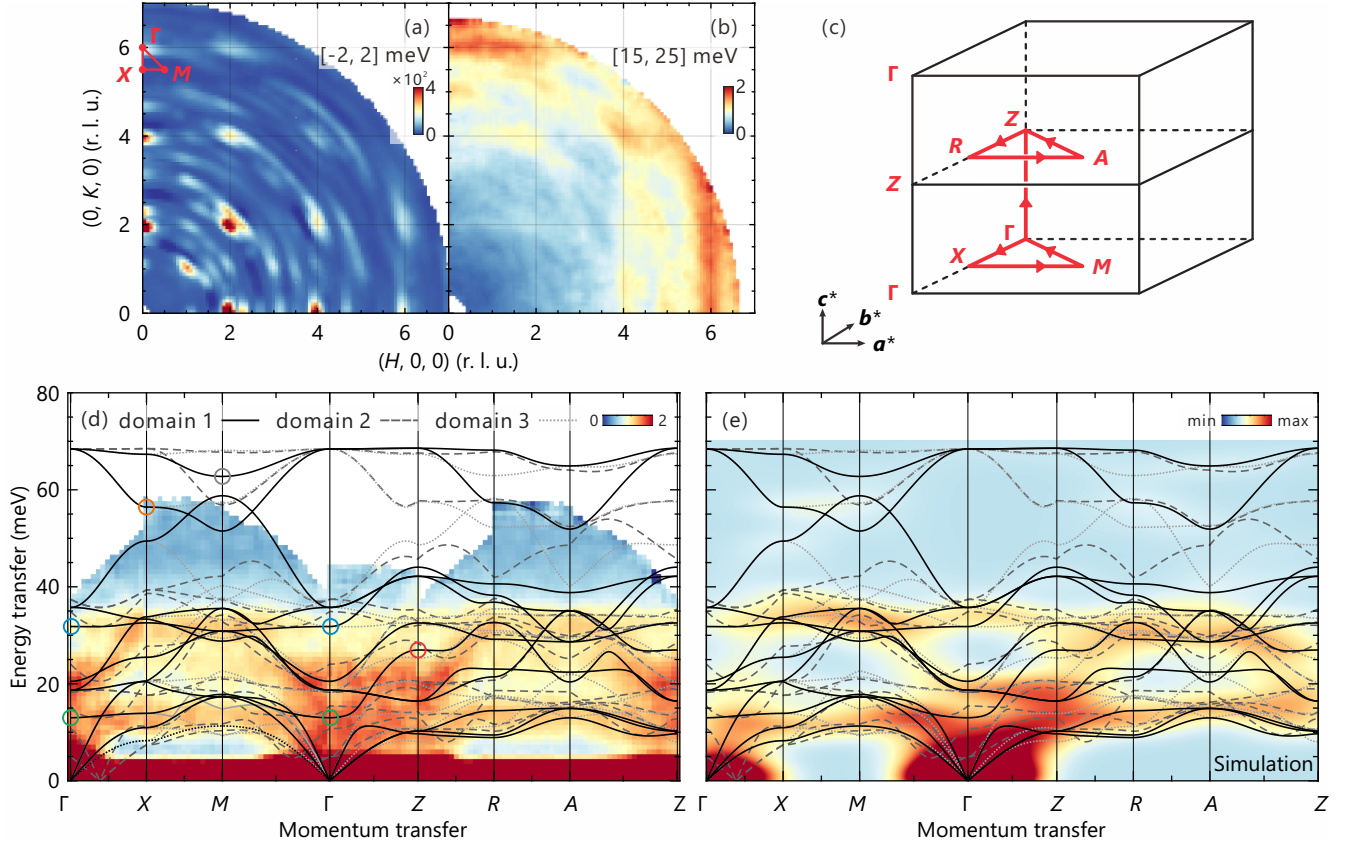


FIG. 3. (a),(b) Constant energy slices of folded INS spectra in the  $(H, K, 0)$  plane for incident energy  $E_i = 76$  meV. The transferred energies are integrated over the following ranges: (a)  $-2 \leq E \leq 2$  meV and (b)  $15 \leq E \leq 25$  meV. A path along high-symmetry points ( $\Gamma$ - $X$ - $M$ - $\Gamma$ ) is illustrated in red color around the (060) Bragg reflection in panel (a). (c) Schematic of a three-dimensional path moving along the high-symmetry points  $\Gamma$ - $X$ - $M$ - $\Gamma$ - $Z$ - $R$ - $A$ - $Z$  according to the tetragonal  $P4/mmm$  unit cell of  $\text{LaNiO}_2$ . (d) INS map along a high-symmetry path from folded data around the (060) and (600) Bragg peaks, acquired with  $E_i = 76$  meV. The integration range along the two orthogonal directions relative to the path is  $\pm 0.2 \text{ \AA}^{-1}$ . The DFPT computed phonon dispersions for the three twin domains of  $\text{LaNiO}_2$  are superimposed as solid (domain 1), dashed (domain 2), and dotted lines (domain 3). The colored circles on the dispersion curves of domain 1 indicate specific phonon modes discussed in the text. (e) Phonon intensities calculated with the Euphonic software package, using the DFPT phonons as input. The intensities are averaged over the three domains, while the indexing of the high-symmetry path refers to domain 1. In addition, Gaussian broadening is applied along both the momentum ( $\Delta Q = 0.92 \text{ \AA}^{-1}$ ) and energy ( $\Delta E = 4.9$  meV) transfer directions. Details about the domain averaging and broadening are given in the Supplementary Information [89].

The INS measurements were conducted at the thermal neutron time-of-flight spectrometer PANTHER (ILL, France) [90] at 1.5 K. The energy of the incident neutron beam was  $E_i = 76$  meV, yielding a Gaussian energy resolution of  $\Delta E = 4.9$  meV at the elastic line. The scattering plane was chosen such that the crystallographic  $ab$  plane was horizontal, although we note that this reference frame applies only to one out of the three orthogonal  $P4/mmm$  twin domains in the sample. An Al grid sample holder without nickelate crystals was measured under the same conditions and the corresponding background signal was subtracted from all INS spectra shown in the following. Data reduction and background subtraction were performed using MANTID [91], and all data were analyzed using HORACE software [92].

To determine the ground-state crystal structures of  $\text{LaNiO}_2$ , density-functional theory (DFT) [93, 94] level

structural relaxations were performed using the Vienna *ab-initio* Simulation Package (VASP) [95–97]. The Perdew-Burke-Ernzerhof version of the generalized gradient approximation (GGA-PBE) [98] was employed, sampling the Brillouin zone (BZ) with a dense  $13 \times 13 \times 15$  Monkhorst-Pack  $k$ -mesh for a unit cell of  $\text{LaNiO}_2$  and a  $6 \times 6 \times 8$   $k$ -mesh for the  $2 \times 2 \times 2$  supercell of  $\text{LaNiO}_2$ . Energy and force convergence criteria were set to  $10^{-8}$  eV and  $0.01 \text{ eV/\AA}$ , respectively. The experimentally determined lattice parameters of  $\text{LaNiO}_2$  were fixed during structural relaxations while atomic positions were fully relaxed. Phonon spectra for  $\text{LaNiO}_2$  compounds were calculated using density functional perturbation theory (DFPT) [85] and post-processed with the Phonopy code [99]. The Euphonic software package [100, 101] was employed to simulate the INS phonon intensities, using the results from the DFPT calculation as an input.



### III. RESULTS

Figures 2(a)-2(d) display neutron scattering intensity maps in the  $(H, K, 0)$  plane acquired with  $E_i = 76$  meV at the PANTHER spectrometer. The  $H, K, L$  indexing refers to the  $\text{LaNiO}_2$  twin domain with the crystallographic  $ab$  plane lying in the scattering plane, denoted as *domain 1* in the following. In the quasi-elastic scattering map in Fig. 2(a) (energy integration range:  $-2 \leq E \leq 2$  meV), Bragg peaks emerge at integer  $H$  and  $K$  positions, exhibiting a rather smeared out intensity distribution. The peaks are particularly intense for even  $H$  and  $K$  values, which is consistent with the structure factor of  $\text{LaNiO}_2$  in the  $P4/mmm$  space group. In addition, satellite peaks occur in proximity to the Bragg peaks at slightly deviating  $H$  and  $K$  values [see inset in Fig. 2(a)]. These peaks originate from the other two twin domains of the tetragonal  $P4/mmm$  space group of  $\text{LaNiO}_2$ , denoted as *domain 2* and *domain 3* in the following. In a previous XRD study on individual  $\text{LaNiO}_2$  crystals, similarly broad Bragg peak intensity profiles and satellite peaks were observed in XRD maps of the  $(H, K, 0)$  plane [86], suggesting that the total mosaicity of the sample array used for the present INS experiment is comparable to that of individual crystals.

In the inelastic scattering map in Fig. 2(b) with energy range  $6 \leq E \leq 10$  meV, pronounced accumulations of spectral weight occur around even  $H$  and  $K$  values, indicating the presence of characteristic low-energy excitations. The intensity of the spectral weight accumulations increases for larger  $Q$ , which is opposite to the trend in the quasi-elastic scattering in Fig. 2(a). This intensity increase for larger  $Q$  suggests that the excitations are likely phonons, due to the normal phonon polarization factor. For energy transfers above 20 meV [Figs. 2(c) and 2(d)], the spectral weight accumulations become less localized and their intensity fades out.

To further investigate the excitations revealed in Figs. 2(b)-2(d), we next inspect an INS intensity map along a high-symmetry path in the BZ, generated from folded data around the (060) and (600) Bragg peaks. Figures 3(a) and 3(b) display the folded quasi-elastic and inelastic scattering maps in the  $(H, K, 0)$  plane, respectively, and Fig. 3(c) shows a schematic of the high-symmetry path within the  $P4/mmm$  unit cell. In the corresponding INS map [Fig. 3(d)], we find that inelastic, dispersive spectral weight emanates from the  $\Gamma$  point, while flat branches extend across wide paths in the BZ around 15 and 30 meV, connecting the  $X$  and  $M$  point as well as the  $R$  and  $A$  point. Additionally, a broad distribution of spectral weight occurs below 30 meV in the region between  $\Gamma$  and  $Z$ .

To corroborate that the observed spectral weight in Fig. 3(d) originates from phonons, we compute the phonon dispersion in  $\text{LaNiO}_2$  using DFPT. As an input for the DFPT calculation, we use the refined lattice parameters of the  $P4/mmm$  unit cell from the INS experiment (see Supplementary Information [89]). Fur-

thermore, since the investigated sample contains three twin domains, we project the computed phonon dispersions of domains 2 and 3 onto the  $\Gamma-X-M-\Gamma-Z-R-A-Z$  path of domain 1. Notably, the superimposed DFPT dispersions of acoustic and optical phonon branches closely match the INS spectral weight distribution in Fig. 3(d), including the steeply dispersing bands emanating from  $\Gamma$  and the relatively flat bands between  $X$  and  $M$  as well as  $R$  and  $A$ . However, while the experimentally observed spectral weight is sharply confined below  $\sim 38$  meV, the DFPT calculations predict several phonon branches extending up to  $\sim 68$  meV.

For a closer comparison between theory and experiment, we simulate the INS phonon intensity of  $\text{LaNiO}_2$  using the Euphonic software package [100, 101], with DFPT-derived eigenenergies and eigenvectors (cf. Fig. 4 below) of the phonons as input. Figure 3(e) displays the resulting simulated intensity map, averaged over all three domains. In addition, adequate Gaussian broadenings were applied in both momentum and energy transfer directions in the map in Fig. 3(e) (for details see Supplementary Information [89]). Notably, the simulation reproduces not only the absence of significant phonon intensity above  $\sim 38$  meV, but also qualitatively captures key features from Fig. 3(d), such as the spectral weight accumulation around the  $\Gamma-Z$  region and the intense flat bands between  $X$  and  $M$  as well as  $R$  and  $A$ .

In general, the diminishing INS intensity observed in  $\text{LaNiO}_2$  above  $\sim 38$  meV can be attributed to several factors, including that the one-phonon scattering cross-section decreases with increasing phonon energy, scaling approximately as  $1/\omega$ , which naturally reduces intensity at higher energies. In addition, the high-energy phonons in  $\text{LaNiO}_2$  predominantly involve oxygen bending and stretching modes with out-of-phase displacements between some of the neighboring oxygen atoms, reducing the net scattering amplitude.

### IV. DISCUSSION

The close agreement between the measured phonon signal and the DFPT results for modes below  $\sim 38$  meV suggests that this theoretical approach quite reliably captures the essential lattice dynamics of  $\text{LaNiO}_2$ . Hence, we next discuss selected DFPT calculated phonon modes in detail, also drawing comparisons to related modes in cuprates, which were intensively investigated by INS [35–41].

A comprehensive overview of the phonon modes in  $\text{LaNiO}_2$  along with the DFPT computed energies is presented in Fig. 4. At the  $\Gamma$  point, the lowest-energy optical phonon exhibits a computed energy of 13.0 meV [green circle in Fig. 3(d)], involving an anti-phase motion between La and Ni ions along the  $c$ -axis direction [Fig. 4(a)]. The dispersion of the mode between  $\Gamma$  and  $X$  is nearly flat, which is reminiscent of the analogous mode in the isostructural IL cuprate  $\text{SrCuO}_2$  [102]. A second

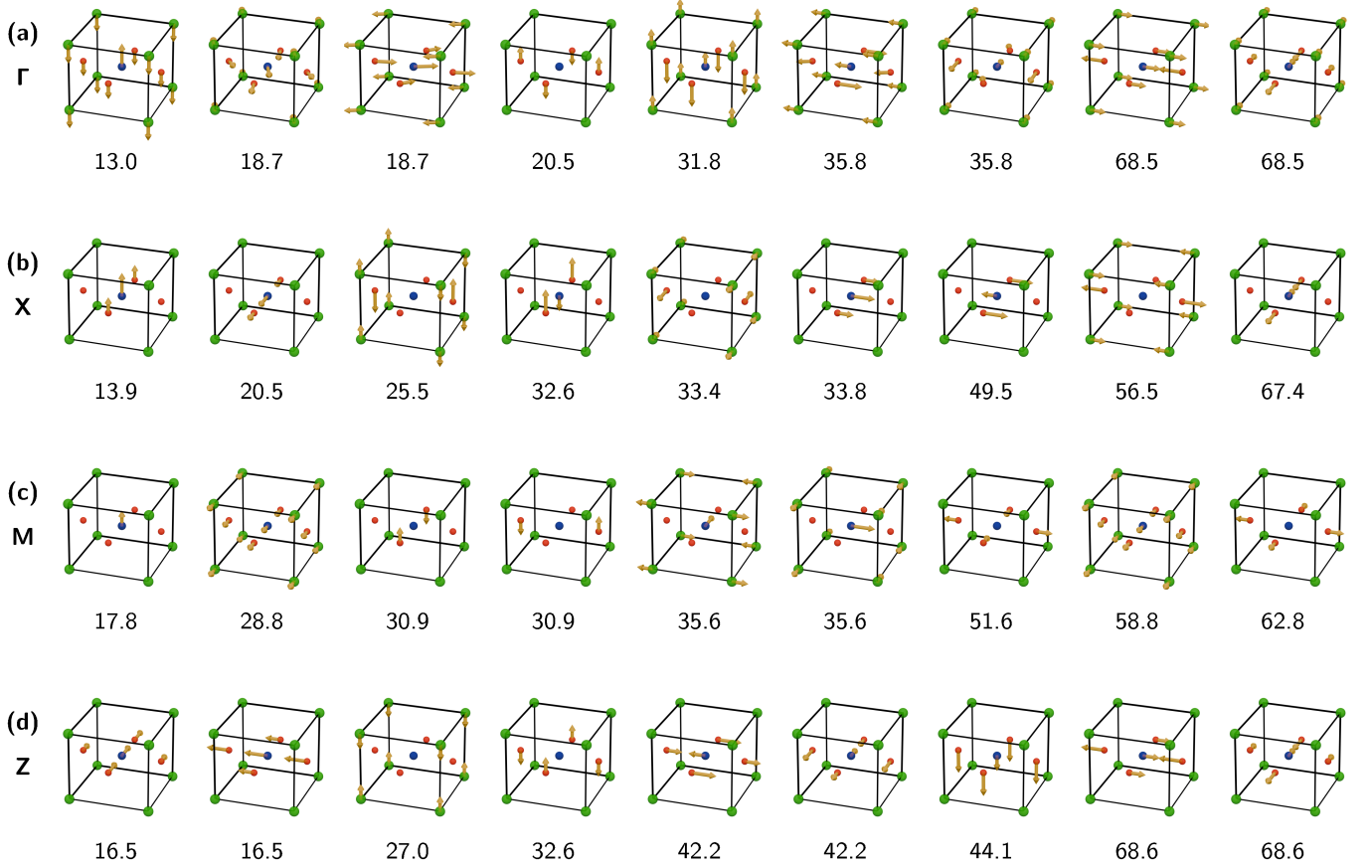


FIG. 4. (a) Atomic displacement patterns of selected phonons of  $\text{LaNiO}_2$  at the  $\Gamma$  point together with the computed phonon energies in units of meV. La atoms are shown in green, Ni in blue, and oxygen in red. The yellow arrows indicate the directions and amplitudes of the atomic vibrations. For clarity, the La, Ni, and O atoms are displayed with reduced atomic radii. (b)-(d) Displacement patterns of phonons at the X, M, and Z points, respectively.

notable  $\Gamma$ -point mode [blue circle in Fig. 3(d)] at 31.8 meV involves in-phase movements of La and Ni against the O atoms [Fig. 4(a)]. This mode also displays minimal dispersion towards X. In cuprates, *ab-initio* rigid-ion model calculations suggest that such modes involving axial displacements of the O sublattice against the cation sublattices can split into longitudinal optical and transverse optical branches [102] and are associated with ferroelectric instabilities. However, this splitting is suppressed under metallic screening conditions [102], consistent with the metallic ground state and absence of ferroelectric behavior in  $\text{LaNiO}_2$  [88].

At the X point, the 56.5 meV phonon [orange circle in Fig. 3(d)] corresponds to the oxygen half-breathing mode (HBM), characterized by the in-plane motion of the O ions along the Ni-O bond direction such that alternating oxygen atoms are displaced towards and away from a central Ni [Fig. 4(b)]. The analogous HBM in the IL cuprate  $\text{SrCuO}_2$  was theoretically described in Ref. [102] and experimentally observed by INS in related cuprates at comparable energies [36], for instance, at 58.5 meV in  $\text{HgBa}_2\text{CuO}_{4+\delta}$  [38]. Interestingly, this longitudinal zone

boundary mode shows strong renormalization effects in doped cuprates below the superconducting transition, underlining the relevance of the HBM also for IL nickelates and warranting future experimental studies with techniques that can resolve the mode.

At the M point, the highest-energy phonon mode, located at 62.8 meV [gray circle in Fig. 3(d)], corresponds to the full-breathing mode (FBM), in which all oxygen ions move uniformly in-phase toward or away from the central Ni ion [Fig. 4(c)]. In cuprates, oxygen breathing distortions, such as the HBM and FBM, are known to be selectively sensitive to the on-site Coulomb repulsion  $U_d$  of the localized Cu 3d orbitals [103–105], with an increased  $U_d$  suppressing charge fluctuations at the Cu site, resulting in a hardening of the breathing mode. In contrast, the smaller  $U_d$  on Ni in IL nickelates generally leads to softer breathing modes compared to their cuprate counterparts. This trend was recently examined in  $\text{LaNiO}_2$  by *ab-initio* many-body methods [80], suggesting that the energy of oxygen breathing modes may serve as an indirect but sensitive probe of electronic correlation strength in this material class.

Notably, the INS map in Fig. 3(d) shows no additional spectral weight around the  $M$  point beyond that attributable to phonons. In particular, we find no indication of spin excitations at the  $M$  point, also not in an analysis focused on small  $\mathbf{Q}$  where the magnetic signal is expected to be strongest (see Supplementary Information [89]). This absence is noteworthy given that the  $M$  point corresponds to the antiferromagnetic zone center in square-lattice Heisenberg antiferromagnets, where a pronounced low-energy magnetic response in this region is well established for cuprates [106]. Moreover, RIXS experiments on IL nickelate thin films [107–109] as well as on  $\text{LaNiO}_2$  crystals from the same synthesis batch [88] have revealed spin excitations consistent with paramagnons arising from  $S = 1/2$  square-lattice Heisenberg-type correlations. This can be explained by our estimate of the expected INS signal strength for spin excitations in IL nickelates (see Supplementary Information [89]), which suggests that a significantly larger sample mass is required to resolve magnetic features in the present experiment.

At the  $Z$  point, the 27.0 meV phonon [red circle in Fig. 3(d)] involves an axial breathing motion of the La ion against the  $\text{NiO}_2$  planes [Fig. 4(d)]. In IL cuprates, the analogous mode has been reported to couple strongly to charge fluctuations [102], typically manifesting as phonon linewidth broadening due to EPC, an effect that has been extensively studied in various cuprate compounds, offering important insights into the interplay between lattice dynamics and electronic correlations [110]. Dynamical interplane charge transfer due to the axial breathing mode is expected to be particularly enhanced in compounds with a short  $c$ -axis lattice parameter [102], such as the recently synthesized Sm-based IL nickelates that might exhibit an enhanced  $T_c$  [111, 112]. In Fig. 3(a), in principle, the broad spectral weight distribution observed between  $\Gamma$  and  $Z$  could result from EPC-induced broadenings, consistent with the predicted presence of strong EPC in IL nickelates [69, 70, 72, 81] and the coupling of certain modes with appropriate symmetry along the  $c$ -direction to charge fluctuations via EPC [102]. However, the limited resolution and statistical quality of our current data preclude an unambiguous assessment of this effect in Fig. 3(d). Future high-resolution INS studies on  $\text{LaNiO}_2$  crystals with higher crystalline quality and a possibly mono-domain character will be necessary to clarify the effect of EPC on certain modes and its general role in IL nickelates.

## V. CONCLUSION

In summary, we have investigated the lattice dynamics of  $\text{LaNiO}_2$  on a sample of co-aligned bulk crystals.

Several branches of acoustic and optical phonons were observed below  $\sim 38$  meV, in good agreement with lattice dynamical calculations based on DFPT. Simulated INS intensity maps, incorporating DFPT mode-resolved eigenvectors and domain averaging, reproduced the main features of the experimental spectra and account for the lack of observable high-energy phonons that are dominated by oxygen displacements and have a low neutron scattering cross-section.

Based on our DFPT results, we have identified and discussed several characteristic phonon modes, including the HBM at the  $X$  point and the FBM at the  $M$  point, which are of particular relevance in the context of related cuprate superconductors. Furthermore, our computational results may also assist in the assignment of infrared-active phonons as well as phonon-induced features observed in other spectroscopic probes such as angle-resolved photoemission spectroscopy [32, 33]. While direct signatures of spin wave excitations and EPC-induced phonon broadening could not be resolved in the present data, such effects may become observable in future high-resolution INS studies on higher-quality and larger-mass  $\text{LaNiO}_2$  crystals. Overall, our results establish an experimental foundation for understanding the lattice dynamics of IL nickelates and lay the groundwork for future investigations addressing electron-phonon interactions, structural instabilities, and their possible relevance to superconductivity in this material class.

## ACKNOWLEDGMENTS

We thank C. Falter and A. Krajewska for insightful discussions. We acknowledge the Institut Laue Langevin (ILL), Grenoble, France for provision of neutron beamtime under the proposal No. 4-02-634 at PANTHER [113]. We thank D. Ueta and T. Yokoo for a preliminary neutron scattering experiment on a test sample performed at the polarized neutron spectrometer POLANO [114] with unpolarized neutrons in the Material and Life Science Experiment Facility (MLF) of the Japan Proton Accelerator Research Complex (J-PARC). The experiment on POLANO was approved by the Neutron Scattering Program Advisory Committee of the Institute of Materials Structure Science, High Energy Accelerator Research Organization, as the S-type research project (2019S09). L. S. acknowledges support from the National Natural Science Foundation of China (Grant No. 12422407); K. H. from the Austrian Science Funds (FWF) Grant DOI 10.55776/I5398.

---

[1] D. Li, K. Lee, B. Y. Wang, M. Osada, S. Crossley, H. R. Lee, Y. Cui, Y. Hikita, and H. Y. Hwang, Supercon-

ductivity in an infinite-layer nickelate, *Nature* **572**, 624

- (2019).
- [2] B. Keimer, S. A. Kivelson, M. R. Norman, S. Uchida, and J. Zaanen, From quantum matter to high-temperature superconductivity in copper oxides, *Nature* **518**, 179 (2015).
  - [3] D. J. Scalapino, A common thread: The pairing interaction for unconventional superconductors, *Rev. Mod. Phys.* **84**, 1383 (2012).
  - [4] N. P. Armitage, P. Fournier, and R. L. Greene, Progress and perspectives on electron-doped cuprates, *Rev. Mod. Phys.* **82**, 2421 (2010).
  - [5] P. A. Lee, N. Nagaosa, and X.-G. Wen, Doping a Mott insulator: Physics of high-temperature superconductivity, *Rev. Mod. Phys.* **78**, 17 (2006).
  - [6] V. I. Anisimov, D. Bukhvalov, and T. M. Rice, Electronic structure of possible nickelate analogs to the cuprates, *Phys. Rev. B* **59**, 7901 (1999).
  - [7] S. Zeng, C. S. Tang, X. Yin, C. Li, M. Li, Z. Huang, J. Hu, W. Liu, G. J. Omar, H. Jani, Z. S. Lim, K. Han, D. Wan, P. Yang, S. J. Pennycook, A. T. S. Wee, and A. Ariando, Phase Diagram and Superconducting Dome of Infinite-Layer  $\text{Nd}_{1-x}\text{Sr}_x\text{NiO}_2$  Thin Films, *Phys. Rev. Lett.* **125**, 147003 (2020).
  - [8] D. Li, B. Y. Wang, K. Lee, S. P. Harvey, M. Osada, B. H. Goodge, L. F. Kourkoutis, and H. Y. Hwang, Superconducting Dome in  $\text{Nd}_{1-x}\text{Sr}_x\text{NiO}_2$  Infinite Layer Films, *Phys. Rev. Lett.* **125**, 027001 (2020).
  - [9] M. Osada, B. Y. Wang, K. Lee, D. Li, and H. Y. Hwang, Phase diagram of infinite layer praseodymium nickelate  $\text{Pr}_{1-x}\text{Sr}_x\text{NiO}_2$  thin films, *Phys. Rev. Mater.* **4**, 121801 (2020).
  - [10] Q. Gao, Y. Zhao, X.-J. Zhou, and Z. Zhu, Preparation of Superconducting Thin Films of Infinite-Layer Nickelate  $\text{Nd}_{0.8}\text{Sr}_{0.2}\text{NiO}_2$ , *Chin. Phys. Lett.* **38**, 077401 (2021).
  - [11] S. Zeng, C. Li, L. E. Chow, Y. Cao, Z. Zhang, C. S. Tang, X. Yin, Z. S. Lim, J. Hu, P. Yang, and A. Ariando, Superconductivity in infinite-layer nickelate  $\text{La}_{1-x}\text{Ca}_x\text{NiO}_2$  thin films, *Sci. Adv.* **8**, eabl9927 (2022).
  - [12] H. Sahib, A. Raji, F. Rosa, G. Merzoni, G. Ghiringhelli, M. Salluzzo, A. Gloter, N. Viart, and D. Preziosi, Superconductivity in  $\text{PrNiO}_2$  Infinite-Layer Nickelates, *Adv. Mater.* **37**, 202416187 (2025).
  - [13] K.-W. Lee and W. E. Pickett, Infinite-layer  $\text{LaNiO}_2$ :  $\text{Ni}^{1+}$  is not  $\text{Cu}^{2+}$ , *Phys. Rev. B* **70**, 165109 (2004).
  - [14] Y. Nomura, M. Hirayama, T. Tadano, Y. Yoshimoto, K. Nakamura, and R. Arita, Formation of a two-dimensional single-component correlated electron system and band engineering in the nickelate superconductor  $\text{NdNiO}_2$ , *Phys. Rev. B* **100**, 205138 (2019).
  - [15] A. S. Botana and M. R. Norman, Similarities and differences between  $\text{LaNiO}_2$  and  $\text{CaCuO}_2$  and implications for superconductivity, *Phys. Rev. X* **10**, 011024 (2020).
  - [16] M. Kitatani, L. Si, O. Janson, R. Arita, Z. Zhong, and K. Held, Nickelate superconductors—a renaissance of the one-band Hubbard model, *npj Quantum Mater.* **5**, 59 (2020), 2002.12230.
  - [17] X. Wu, D. Di Sante, T. Schwemmer, W. Hanke, H. Y. Hwang, S. Raghu, and R. Thomale, Robust  $d_{x^2-y^2}$ -wave superconductivity of infinite-layer nickelates, *Phys. Rev. B* **101**, 060504 (2020).
  - [18] H. Zhang, L. Jin, S. Wang, B. Xi, X. Shi, F. Ye, and J.-W. Mei, Effective hamiltonian for nickelate oxides  $\text{Nd}_{1-x}\text{Sr}_x\text{NiO}_2$ , *Phys. Rev. Research* **2**, 013214 (2020).
  - [19] H. Sakakibara, H. Usui, K. Suzuki, T. Kotani, H. Aoki, and K. Kuroki, Model construction and a possibility of cupratelike pairing in a new  $d^9$  nickelate superconductor  $(\text{Nd}, \text{Sr})\text{NiO}_2$ , *Phys. Rev. Lett.* **125**, 077003 (2020).
  - [20] F. Lechermann, Late transition metal oxides with infinite-layer structure: Nickelates versus cuprates, *Phys. Rev. B* **101**, 081110 (2020).
  - [21] Y. Wang, C.-J. Kang, H. Miao, and G. Kotliar, Hund’s metal physics: From  $\text{SrNiO}_2$  to  $\text{LaNiO}_2$ , *Phys. Rev. B* **102**, 161118 (2020).
  - [22] P. Werner and S. Hoshino, Nickelate superconductors: Multiorbital nature and spin freezing, *Phys. Rev. B* **101**, 041104 (2020).
  - [23] J. Karp, A. S. Botana, M. R. Norman, H. Park, M. Zingl, and A. Millis, Many-body electronic structure of  $\text{NdNiO}_2$  and  $\text{CaCuO}_2$ , *Phys. Rev. X* **10**, 021061 (2020).
  - [24] Z. Liu, C. Xu, C. Cao, W. Zhu, Z. F. Wang, and J. Yang, Doping dependence of electronic structure of infinite-layer  $\text{NdNiO}_2$ , *Phys. Rev. B* **103**, 045103 (2021).
  - [25] X. Wan, V. Ivanov, G. Resta, I. Leonov, and S. Y. Savrasov, Exchange interactions and sensitivity of the  $n_i$  two-hole spin state to hund’s coupling in doped  $\text{NdNiO}_2$ , *Phys. Rev. B* **103**, 075123 (2021).
  - [26] Z.-J. Lang, R. Jiang, and W. Ku, Strongly correlated doped hole carriers in the superconducting nickelates: Their location, local many-body state, and low-energy effective hamiltonian, *Phys. Rev. B* **103**, L180502 (2021).
  - [27] K. Higashi, M. Winder, J. Kuneš, and A. Hariki, Core-level x-ray spectroscopy of infinite-layer nickelate: LDA + DMFT study, *Phys. Rev. X* **11**, 041009 (2021).
  - [28] K. Held, L. Si, P. Worm, O. Janson, R. Arita, Z. Zhong, J. Tomczak, and M. Kitatani, Phase diagram of nickelate superconductors calculated by dynamical vertex approximation, *Front. Phys.* **9**:810394 (2022).
  - [29] H. Chen, A. Hampel, J. Karp, F. Lechermann, and A. Millis, Dynamical mean field studies of infinite layer nickelates: Physics results and methodological implications, *Front. Phys.* **10**:835942 (2022).
  - [30] M. Hepting, D. Li, C. J. Jia, H. Lu, E. Paris, Y. Tseng, X. Feng, M. Osada, E. Been, Y. Hikita, Y.-D. Chuang, Z. Hussain, K. J. Zhou, A. Nag, M. Garcia-Fernandez, M. Rossi, H. Y. Huang, D. J. Huang, Z. X. Shen, T. Schmitt, H. Y. Hwang, B. Moritz, J. Zaanen, T. P. Devereaux, and W. S. Lee, Electronic structure of the parent compound of superconducting infinite-layer nickelates, *Nat. Mater.* **19**, 381 (2020).
  - [31] B. H. Goodge, D. Li, K. Lee, M. Osada, B. Y. Wang, G. A. Sawatzky, H. Y. Hwang, and L. F. Kourkoutis, Doping evolution of the mott–hubbard landscape in infinite-layer nickelates, *PNAS* **118**, e2007683118 (2021).
  - [32] X. Ding, Y. Fan, X. Wang, C. Li, Z. An, J. Ye, S. Tang, M. Lei, X. Sun, N. Guo, Z. Chen, S. Sangphet, Y. Wang, H. Xu, R. Peng, and D. Feng, Cuprate-like electronic structures in infinite-layer nickelates with substantial hole dopings, *Natl. Sci. Rev.* **11**, nwae194 (2024).
  - [33] W. Sun, Z. Jiang, C. Xia, B. Hao, S. Yan, M. Wang, Y. Li, H. Liu, J. Ding, J. Liu, Z. Liu, J. Liu, H. Chen, D. Shen, and Y. Nie, Electronic structure of superconducting infinite-layer lanthanum nickelates, *Sci. Adv.* **11**, eadr5116 (2025).
  - [34] L. Pintschovius, N. Pyka, W. Reichardt, A. Rumiantsev, N. Mitrofanov, A. Ivanov, G. Collin, and P. Bourges,



- Lattice dynamical studies of HTSC materials, *Physica C: Superconductivity* **185-189**, 156 (1991).
- [35] H. F. Fong, B. Keimer, P. W. Anderson, D. Reznik, F. Doğan, and I. A. Aksay, Phonon and Magnetic Neutron Scattering at 41 meV in  $\text{YBa}_2\text{Cu}_3\text{O}_7$ , *Phys. Rev. Lett.* **75**, 316 (1995).
  - [36] D. Reznik, L. Pintschovius, J. M. Tranquada, M. Arai, Y. Endoh, T. Masui, and S. Tajima, Temperature dependence of the bond-stretching phonon anomaly in  $\text{YBa}_2\text{Cu}_3\text{O}_{6.95}$ , *Phys. Rev. B* **78**, 094507 (2008).
  - [37] M. Raichle, D. Reznik, D. Lamago, R. Heid, Y. Li, M. Bakr, C. Ulrich, V. Hinkov, K. Hradil, C. T. Lin, and B. Keimer, Highly Anisotropic Anomaly in the Dispersion of the Copper-Oxygen Bond-Bending Phonon in Superconducting  $\text{YBa}_2\text{Cu}_3\text{O}_7$  from Inelastic Neutron Scattering, *Phys. Rev. Lett.* **107**, 177004 (2011).
  - [38] I. Ahmadova, T. C. Sterling, A. C. Sokolik, D. L. Abernathy, M. Greven, and D. Reznik, Phonon spectrum of underdoped  $\text{HgBa}_2\text{CuO}_{4+\delta}$  investigated by neutron scattering, *Phys. Rev. B* **101**, 184508 (2020).
  - [39] T. C. Sterling and D. Reznik, Effect of the electronic charge gap on LO bond-stretching phonons in undoped  $\text{La}_2\text{CuO}_4$  calculated using LDA + U, *Phys. Rev. B* **104**, 134311 (2021).
  - [40] W. Reichardt, J. Peisl, P. Schweiss, A. Boriws, G. Collin, R.-M. Y., H. N.S., I. N.L., M. V.A., and Rumyantsev, Anharmonicity and electron-phonon coupling in cuprate superconductors studied by inelastic neutron scattering, *Journal of Superconductivity* **6**, 397 (1993).
  - [41] L. Pintschovius, Electron-phonon coupling effects explored by inelastic neutron scattering, *phys. stat. sol. (b)* **242**, 30 (2005).
  - [42] A. Frano, S. Blanco-Canosa, B. Keimer, and R. J. Birgeneau, Charge ordering in superconducting copper oxides, *J. Phys.: Condens. Matter* **32**, 374005 (2020).
  - [43] M. Le Tacon, G. Ghiringhelli, J. Chaloupka, M. M. Sala, V. Hinkov, M. W. Haverkort, M. Minola, M. Bakr, K. J. Zhou, S. Blanco-Canosa, C. Monney, Y. T. Song, G. L. Sun, C. T. Lin, G. M. De Luca, M. Salluzzo, G. Khal-iullin, T. Schmitt, L. Braicovich, and B. Keimer, Intense paramagnon excitations in a large family of high-temperature superconductors, *Nat. Phys.* **7**, 725 (2011).
  - [44] M. P. M. Dean, G. Dellea, R. S. Springell, F. Yakhour-Harris, K. Kummer, N. B. Brookes, X. Liu, Y.-J. Sun, J. Strle, T. Schmitt, L. Braicovich, G. Ghiringhelli, I. Božović, and J. P. Hill, Persistence of magnetic excitations in  $\text{La}_{2-x}\text{Sr}_x\text{CuO}_4$  from the undoped insulator to the heavily overdoped non-superconducting metal, *Nat. Mater.* **12**, 1019 (2013).
  - [45] P. A. Lee, N. Nagaosa, and X.-G. Wen, Doping a mott insulator: Physics of high-temperature superconductivity, *Rev. Mod. Phys.* **78**, 17 (2006).
  - [46] D. J. Scalapino, A common thread: The pairing interaction for unconventional superconductors, *Rev. Mod. Phys.* **84**, 1383 (2012).
  - [47] P. Dai, H. A. Mook, R. D. Hunt, and F. Doğan, Evolution of the resonance and incommensurate spin fluctuations in superconducting  $\text{YBa}_2\text{Cu}_3\text{O}_{6+x}$ , *Phys. Rev. B* **63**, 054525 (2001).
  - [48] D. Vilardi, C. Taranto, and W. Metzner, Antiferromagnetic and  $d$ -wave pairing correlations in the strongly interacting two-dimensional hubbard model from the functional renormalization group, *Phys. Rev. B* **99**, 104501 (2019).
  - [49] T. Cuk, F. Baumberger, D. H. Lu, N. Ingle, X. J. Zhou, H. Eisaki, N. Kaneko, Z. Hussain, T. P. Devereaux, N. Nagaosa, and Z.-X. Shen, Coupling of the  $B_{1g}$  Phonon to the Antinodal Electronic States of  $\text{Bi}_2\text{Sr}_2\text{Ca}_{0.92}\text{Y}_{0.08}\text{Cu}_2\text{O}_{8+\delta}$ , *Phys. Rev. Lett.* **93**, 117003 (2004).
  - [50] R. Heid, R. Zeyher, D. Manske, and K.-P. Bohnen, Phonon-induced pairing interaction in  $\text{YBa}_2\text{Cu}_3\text{O}_7$  within the local-density approximation, *Phys. Rev. B* **80**, 024507 (2009).
  - [51] F. Giustino, M. L. Cohen, and S. G. Louie, Small phonon contribution to the photoemission kink in the copper oxide superconductors, *Nature* **452**, 975 (2008).
  - [52] D. Reznik, G. Sangiovanni, O. Gunnarsson, and T. P. Devereaux, Photoemission kinks and phonons in cuprates, *Nature* **455**, E6 (2008).
  - [53] S. Johnston, F. Vernay, B. Moritz, Z.-X. Shen, N. Nagaosa, J. Zaanen, and T. P. Devereaux, Systematic study of electron-phonon coupling to oxygen modes across the cuprates, *Phys. Rev. B* **82**, 064513 (2010).
  - [54] T. Bauer and C. Falter, Impact of dynamical screening on the phonon dynamics of metallic  $\text{La}_2\text{CuO}_4$ , *Phys. Rev. B* **80**, 094525 (2009).
  - [55] S. P. Harvey, B. Y. Wang, J. Fowlie, M. Osada, K. Lee, Y. Lee, D. Li, and H. Y. Hwang, Evidence for nodal superconductivity in infinite-layer nickelates, (2022), [arXiv:2201.12971 \[cond-mat.supr-con\]](https://arxiv.org/abs/2201.12971).
  - [56] L. E. Chow, S. K. Sudheesh, Z. Y. Luo, P. Nandi, T. Heil, J. Deusche, S. W. Zeng, Z. T. Zhang, S. Prakash, X. M. Du, Z. S. Lim, P. A. van Aken, E. E. M. Chia, and A. Ariando, Pairing symmetry in infinite-layer nickelate superconductor, (2022), [arXiv:2201.10038 \[cond-mat.supr-con\]](https://arxiv.org/abs/2201.10038).
  - [57] Q. Gu, Y. Li, S. Wan, H. Li, W. Guo, H. Yang, Q. Li, X. Zhu, X. Pan, Y. Nie, and H.-H. Wen, Single particle tunneling spectrum of superconducting  $\text{Nd}_{1-x}\text{Sr}_x\text{NiO}_2$  thin films, *Nat. Commun.* **11**, 6027 (2020).
  - [58] R.-F. Wang, Y.-L. Xiong, H. Yan, X. Hu, M. Osada, D. Li, H. Y. Hwang, C.-L. Song, X.-C. Ma, and Q.-K. Xue, Observation of Coulomb blockade and Coulomb staircases in superconducting  $\text{Pr}_{0.8}\text{Sr}_{0.2}\text{NiO}_2$  films, *Phys. Rev. B* **107**, 115411 (2023).
  - [59] P. Choubey and I. M. Eremin, Electronic theory for scanning tunneling microscopy spectra in infinite-layer nickelate superconductors, *Phys. Rev. B* **104**, 144504 (2021).
  - [60] A. Kreisel, B. M. Andersen, A. T. Rømer, I. M. Eremin, and F. Lechermann, Superconducting instabilities in strongly correlated infinite-layer nickelates, *Phys. Rev. Lett.* **129**, 077002 (2022).
  - [61] B. Cheng, D. Cheng, K. Lee, L. Luo, Z. Chen, Y. Lee, B. Y. Wang, M. Mootz, I. E. Perakis, Z.-X. Shen, H. Y. Hwang, and J. Wang, Evidence for  $d$ -wave superconductivity of infinite-layer nickelates from low-energy electrodynamics, *Nat. Mater.* **23**, 775 (2024).
  - [62] A. Schilling, M. Cantoni, J. D. Guo, and H. R. Ott, Superconductivity above 130 K in the Hg-Ba-Ca-Cu-O system, *Nature* **363**, 56 (1993).
  - [63] K. Lee, B. Y. Wang, M. Osada, B. H. Goodge, T. C. Wang, Y. Lee, S. Harvey, W. J. Kim, Y. Yu, C. Murthy, S. Raghu, L. F. Kourkoutis, and H. Y. Hwang, Linear-in-temperature resistivity for optimally superconducting  $(\text{Nd},\text{Sr})\text{NiO}_2$ , *Nature* **619**, 288 (2023).



- [64] C. Xia, J. Wu, Y. Chen, and H. Chen, Dynamical structural instability and its implications for the physical properties of infinite-layer nickelates, *Phys. Rev. B* **105**, 115134 (2022).
- [65] A. A. Carrasco Álvarez, S. Petit, L. Iglesias, W. Prellier, M. Bibes, and J. Varignon, Structural instabilities of infinite-layer nickelates from first-principles simulations, *Phys. Rev. Res.* **4**, 023064 (2022).
- [66] Y. Zhang, J. Zhang, J. Li, M. P. K. Sahoo, X. He, J. Wang, and P. Ghosez, Displacive phase transitions in infinite-layer nickelates from first- and second-principles calculations, *Phys. Rev. B* **108**, 165117 (2023).
- [67] Q. N. Meier, J. B. de Vaulx, F. Bernardini, A. S. Botana, X. Blase, V. Olevano, and A. Cano, Preempted phonon-mediated superconductivity in the infinite-layer nickelates, *Phys. Rev. B* **109**, 184505 (2024).
- [68] H. Sakakibara, R. Mizuno, M. Ochi, H. Usui, and K. Kuroki, Theoretical study on the possibility of high  $T_c$   $s^{\pm}$ -wave superconductivity in the heavily hole-doped infinite layer nickelates, (2024), [arXiv:2407.21461](https://arxiv.org/abs/2407.21461) [cond-mat.supr-con].
- [69] R. Zhang, C. Lane, J. Nokelainen, B. Singh, B. Barbiellini, R. S. Markiewicz, A. Bansil, and J. Sun, Emergence of Competing Stripe Phases in Undoped Infinite-Layer Nickelates, *Phys. Rev. Lett.* **133**, 066401 (2024).
- [70] Z. Li and S. G. Louie, Two-Gap Superconductivity and the Decisive Role of Rare-Earth  $d$  Electrons in Infinite-Layer Nickelates, *Phys. Rev. Lett.* **133**, 126401 (2024).
- [71] A. A. Carrasco Álvarez, L. Iglesias, S. Petit, W. Prellier, M. Bibes, and J. Varignon, Charge ordering as the driving mechanism for superconductivity in rare-earth nickel oxides, *Phys. Rev. Mater.* **8**, 064801 (2024).
- [72] X. Sui, J. Wang, C. Chen, X. Ding, K.-J. Zhou, C. Cao, L. Qiao, H. Lin, and B. Huang, Hole doping dependent electronic instability and electron-phonon coupling in infinite-layer nickelates, *Phys. Rev. B* **107**, 075159 (2023).
- [73] L. Craco, Orbital-Nematic and Two-Fluid Superconductivity in Hole-Doped  $\text{NdNiO}_2$ , *Condens. Matter* **10** (2025).
- [74] S. Di Cataldo, P. Worm, L. Si, and K. Held, Absence of electron-phonon-mediated superconductivity in hydrogen-intercalated nickelates, *Phys. Rev. B* **108**, 174512 (2023).
- [75] X. Wu, D. Di Sante, T. Schwemmer, W. Hanke, H. Y. Hwang, S. Raghu, and R. Thomale, Robust  $d_{x^2-y^2}$ -wave superconductivity of infinite-layer nickelates, *Phys. Rev. B* **101**, 060504 (2020).
- [76] M. Kitatani, L. Si, P. Worm, J. M. Tomczak, R. Arita, and K. Held, Optimizing Superconductivity: From Cuprates via Nickelates to Palladates, *Phys. Rev. Lett.* **130**, 166002 (2023).
- [77] P. Adhikary, S. Bandyopadhyay, T. Das, I. Dasgupta, and T. Saha-Dasgupta, Orbital-selective superconductivity in a two-band model of infinite-layer nickelates, *Phys. Rev. B* **102**, 100501 (2020).
- [78] L. Si, P. Worm, D. Chen, and K. Held, Topotactic hydrogen forms chains in  $\text{ABO}_2$  nickelate superconductors, *Phys. Rev. B* **107**, 165116 (2023).
- [79] S. Sharma, M.-C. Jung, H. LaBollita, and A. S. Botana, Pressure effects on the electronic structure and magnetic properties of infinite-layer nickelates, *Phys. Rev. B* **110**, 155156 (2024).
- [80] Y. Wang, Hardening of Ni-O bond-stretching phonons in  $\text{LaNiO}_2$ , *Phys. Rev. B* **111**, 085117 (2025).
- [81] R. Zhang, Y. Wang, M. Engel, C. Lane, H. Miranda, L. Hou, S. Chowdhury, B. Singh, B. Barbiellini, J.-X. Zhu, *et al.*, Magnetism-enhanced strong electron-phonon coupling in infinite-layer nickelate, (2025), [arXiv:2504.13025](https://arxiv.org/abs/2504.13025) [cond-mat.str-el].
- [82] R. Cervasio, L. Tomarchio, M. Verseils, J.-B. Brubach, S. Macis, S. Zeng, A. Ariando, P. Roy, and S. Lupi, Optical Properties of Superconducting  $\text{Nd}_{0.8}\text{Sr}_{0.2}\text{NiO}_2$  Nickelate, *ACS Appl. Electron. Mater.* **5**, 4770 (2023).
- [83] G. Burns, M. K. Crawford, F. H. Dacol, E. M. McCarron, and T. M. Shaw, Phonons in  $\text{CaCuO}_2$ , *Phys. Rev. B* **40**, 6717 (1989).
- [84] P. Puphal, Y.-M. Wu, K. Fürsich, H. Lee, M. Pakdaman, J. A. N. Bruin, J. Nuss, Y. E. Suyolcu, P. A. van Aken, B. Keimer, M. Isobe, and M. Hepting, Topotactic transformation of single crystals: From perovskite to infinite-layer nickelates, *Sci. Adv.* **7**, eabl8091 (2021).
- [85] S. Baroni, S. de Gironcoli, A. Dal Corso, and P. Giannozzi, Phonons and related crystal properties from density-functional perturbation theory, *Rev. Mod. Phys.* **73**, 515 (2001).
- [86] P. Puphal, B. Wehinger, J. Nuss, K. Küster, U. Starke, G. Garbarino, B. Keimer, M. Isobe, and M. Hepting, Synthesis and physical properties of  $\text{LaNiO}_2$  crystals, *Phys. Rev. Mater.* **7**, 014804 (2023).
- [87] P. Puphal, V. Sundaramurthy, V. Zimmermann, K. Küster, U. Starke, M. Isobe, B. Keimer, and M. Hepting, Phase formation in hole- and electron-doped rare-earth nickelate single crystals, *APL Mater.* **11**, 081107 (2023).
- [88] S. Hayashida, V. Sundaramurthy, P. Puphal, M. Garcia-Fernandez, K.-J. Zhou, B. Fenk, M. Isobe, M. Minola, Y.-M. Wu, Y. E. Suyolcu, P. A. van Aken, B. Keimer, and M. Hepting, Investigation of spin excitations and charge order in bulk crystals of the infinite-layer nickelate  $\text{LaNiO}_2$ , *Phys. Rev. B* **109**, 235106 (2024).
- [89] See Supplemental Material for the complementary inelastic neutron scattering spectra of  $\text{LaNiO}_2$  crystals. The Supplemental Material also contains Refs. [86, 88, 100, 101, 107].
- [90] B. Fåk, S. Rols, G. Manzin, and O. Meulien, Panther — the new thermal neutron time-of-flight spectrometer at the ILL, *EPJ Web Conf.* **272**, 7 (2022).
- [91] O. Arnold, J. Bilheux, J. Borreguero, A. Buts, S. Campbell, L. Chapon, M. Doucet, N. Draper, R. Ferraz Leal, M. Gigg, V. Lynch, A. Markvardsen, D. Mikkelsen, R. Mikkelsen, R. Miller, K. Palmen, P. Parker, G. Passos, T. Perring, P. Peterson, S. Ren, M. Reuter, A. Savici, J. Taylor, R. Taylor, R. Tolchenov, W. Zhou, and J. Zikovsky, Mantid—Data analysis and visualization package for neutron scattering and  $\mu\text{SR}$  experiments, *Nucl. Instrum. Methods Phys. Res. A* **764**, 156 (2014).
- [92] R. Ewings, A. Buts, M. Le, J. van Duijn, I. Bustinduy, and T. Perring, Horace: Software for the analysis of data from single crystal spectroscopy experiments at time-of-flight neutron instruments, *Nucl. Instrum. Methods Phys. Res. A* **834**, 132 (2016).
- [93] P. Hohenberg and W. Kohn, Inhomogeneous electron gas, *Phys. Rev.* **136**, B864 (1964).
- [94] W. Kohn and L. J. Sham, Self-consistent equations including exchange and correlation effects, *Phys. Rev.*

- 140**, A1133 (1965).
- [95] G. Kresse and J. Fürthmüller, Efficiency of ab-initio total energy calculations for metals and semiconductors using a plane-wave basis set, *Comput. Mater. Sci.* **6**, 15 (1996).
  - [96] G. Kresse and J. Fürthmüller, Efficient iterative schemes for ab initio total-energy calculations using a plane-wave basis set, *Phys. Rev. B* **54**, 11169 (1996).
  - [97] G. Kresse and D. Joubert, From ultrasoft pseudopotentials to the projector augmented-wave method, *Phys. Rev. B* **59**, 1758 (1999).
  - [98] J. P. Perdew, K. Burke, and M. Ernzerhof, Generalized gradient approximation made simple, *Phys. Rev. Lett.* **77**, 3865 (1996).
  - [99] A. Togo and I. Tanaka, First principles phonon calculations in materials science, *Scripta Materialia* **108**, 1 (2015).
  - [100] R. L. Fair, J. L. Farmer, A. J. Jackson, J. C. King, M. D. Le, T. G. Perring, C. Pettitt, K. Refson, G. S. Tucker, D. J. Voneshen, and J. S. Wilkins, *Euphonic*.
  - [101] R. Fair, A. Jackson, D. Voneshen, D. Jochym, D. Le, K. Refson, and T. Perring, *Euphonic*: inelastic neutron scattering simulations from force constants and visualization tools for phonon properties, *J. Appl. Cryst.* **55**, 1689 (2022).
  - [102] M. Klenner, C. Falter, and Q. Chen, Calculated phonon dispersion of infinite-layer compounds and the effects of charge fluctuations, *Z. Phys. B* **95**, 417 (1994).
  - [103] C. Falter, M. Klenner, and W. Ludwig, Effect of charge fluctuations on the phonon dispersion and electron-phonon interaction in  $\text{La}_2\text{CuO}_4$ , *Phys. Rev. B* **47**, 5390 (1993).
  - [104] C. Falter, M. Klenner, G. A. Hoffmann, and Q. Chen, Origin of phonon anomalies in  $\text{La}_2\text{CuO}_4$ , *Phys. Rev. B* **55**, 3308 (1997).
  - [105] C. Falter, T. Bauer, and F. Schnetgöke, Modeling the electronic state of the high- $T_c$  superconductor  $\text{LaCuO}$ : Phonon dynamics and charge response, *Phys. Rev. B* **73**, 224502 (2006).
  - [106] R. J. Birgeneau, C. Stock, J. M. Tranquada, and K. Yamada, Magnetic neutron scattering in hole-doped cuprate superconductors, *J. Phys. Soc. Jpn.* **75**, 111003 (2006).
  - [107] H. Lu, M. Rossi, A. Nag, M. Osada, D. F. Li, K. Lee, B. Y. Wang, M. Garcia-Fernandez, S. Agrestini, Z. X. Shen, E. M. Been, B. Moritz, T. P. Devereaux, J. Zaanen, H. Y. Hwang, K.-J. Zhou, and W. S. Lee, Magnetic excitations in infinite-layer nickelates, *Science* **373**, 213 (2021).
  - [108] C. C. Tam, J. Choi, X. Ding, S. Agrestini, A. Nag, M. Wu, B. Huang, H. Luo, P. Gao, M. García-Fernández, L. Qiao, and K.-J. Zhou, Charge density waves in infinite-layer  $\text{NdNiO}_2$  nickelates, *Nat. Mater.* **21**, 1116 (2022).
  - [109] G. Krieger, L. Martinelli, S. Zeng, L. E. Chow, K. Kummer, R. Arpaia, M. Moretti Sala, N. B. Brookes, A. Ariando, N. Viart, M. Salluzzo, G. Ghiringhelli, and D. Preziosi, Charge and Spin Order Dichotomy in  $\text{NdNiO}_2$  Driven by the Capping Layer, *Phys. Rev. Lett.* **129**, 027002 (2022).
  - [110] P. Zhang, S. G. Louie, and M. L. Cohen, Electron-Phonon Renormalization in Cuprate Superconductors, *Phys. Rev. Lett.* **98**, 067005 (2007).
  - [111] S. L. E. Chow, Z. Luo, and A. Ariando, Bulk superconductivity near 40 K in hole-doped  $\text{SmNiO}_2$  at ambient pressure, *Nature* (2025).
  - [112] M. Yang, H. Wang, J. Tang, J. Luo, X. Wu, R. Mao, W. Xu, G. Zhou, Z. Dong, B. Feng, L. Shi, Z. Pei, P. Gao, Z. Chen, and D. Li, Enhanced superconductivity in co-doped infinite-layer samarium nickelate thin films, [arXiv:2503.18346 \[cond-mat.supr-con\]](https://arxiv.org/abs/2503.18346).
  - [113] S. Hayashida, B. FÅK, M. Hepting, B. Keimer, T. Keller, A. Krajewska, P. Puphal, and V. Sundaramurthy, Spin dynamics in single-crystals of the infinite-layer-nickelate  $\text{LaNiO}_2$ , Institut Laue-Langevin (ILL) [doi:10.5291/ILL-DATA.4-02-634](https://doi.org/10.5291/ILL-DATA.4-02-634).
  - [114] T. Yokoo, K. Ohoyama, S. Itoh, J. Suzuki, K. Iwasa, T. J. Sato, H. Kira, Y. Sakaguchi, T. Ino, T. Oku, K. Tomiyasu, M. Matsuura, H. Hiraka, M. Fujita, H. Kimura, T. Sato, M. Takeda, K. Kaneko, M. Hino, and S. Muto, Newly Proposed Inelastic Neutron Spectrometer POLANO, *J. Phys. Soc. Jpn.* **82**, SA035 (2013).